

2019 | 314

## Ignition Concepts for Large-Bore Gas Engines – A Comparison of Spark, Laser and Diesel Pilot Ignition

11 - Basic Research & Advanced Engineering - Technologies, Materials & Tools for Future Engines

Jan Zelenka, LEC GmbH

Gerhard Pirker, LEC GmbH

Constantin Kiesling, LEC GmbH

Lucas Eder, LEC GmbH

Hubert Winter, LEC GmbH

Georg Meyer, Hoerbiger Wien GmbH

Andreas Wimmer, LEC GmbH / Graz University of Technology

---

This paper has been presented and published at the 29th CIMAC World Congress 2019 in Vancouver, Canada. The CIMAC Congress is held every three years, each time in a different member country. The Congress program centres around the presentation of Technical Papers on engine research and development, application engineering on the original equipment side and engine operation and maintenance on the end-user side. The themes of the 2019 event included Digitalization & Connectivity for different applications, System Integration, Electrification & Hybridization, Emission Reduction Technologies, Low Carbon Combustion including Global Sulphur Cap 2020, Case Studies from Operators, Product Development of Gas and Diesel Engines, Components & Tribology, Turbochargers, Controls & Automation, Fuels & Lubricants as well as Basic Research & Advanced Engineering. The copyright of this paper is with CIMAC. For further information please visit <https://www.cimac.com>.

## **ABSTRACT**

The majority of modern large bore gas engines are operated using a lean combustion concept to comply with existing NO<sub>x</sub> emission limits without exhaust aftertreatment. Prospective emission regulations call for significantly lower NO<sub>x</sub> emissions. Engine internal measures to achieve this goal include further enleanment of the cylinder charge and high EGR ratios. Exhaust gas aftertreatment increases the size of the engine system; greater power output compensates for the demand for more space. High specific engine power, very lean mixtures or high EGR ratios pose high demands to the ignition of the mixture.

This paper compares the potentials of three different ignition concepts (spark ignition, laser ignition and diesel pilot ignition) applied to large engines. First, the basics of the ignition concepts are compared by theoretical considerations with respect to available ignition energy and temperature, introduced turbulence and stochastic influences.

Measurements from the single cylinder research engine are used to evaluate the influence of the ignition source based on the achievable efficiency and emissions values. Furthermore, the impact on cycle-to-cycle variations is assessed. When the ignition systems are compared, the boundary conditions of the cases under investigation are set to identical values whenever possible.

Finally, the measurement results are further analyzed based on 3D CFD simulation. Highly sophisticated simulation models already validated in prior research are applied in order to simulate the processes relevant to ignition, flame kernel development and combustion. For the modeling of spark ignition, a spherical ignition model is used providing a defined initial flame kernel at the spark plug over the duration of energy deposit by the ignition system. Laser ignition is considered by an ignition model that generates an infant flame kernel represented by a sphere inside the combustion chamber. The size of the sphere is provided by a detailed plasma model for the blast wave resulting from the instantaneous energy release by the focused laser beam. Finally, for diesel pilot ignition a detailed reaction mechanism is used to obtain the relevant ignition delay values. The models are used in connection with 3D CFD simulation, which also provides the required turbulence values. The effect of each ignition concept on the induced energy to the cylinder charge as well as on the evolution of the initial flame front is investigated.

## 1 INTRODUCTION

Large gas engines play an important role in future scenarios of a decentralized energy supply due to their high efficiency and comparably low emissions [1], [2]. Natural gas has significantly higher reserves than other fossil fuels, and waste gases from industrial processes can also be used as valuable fuel gases.

The significant increase in the efficiency of large gas engines that has occurred in recent years has been achieved with highly advanced combustion systems and ignition concepts that employ high mean effective pressures and extremely lean gas-air mixtures in combination with very early inlet valve closing to reduce the tendency for knock and the formation of nitrogen oxide emissions [3]. A significantly increased excess air ratio also results in a high cylinder pressure at the ignition timing. Ideally, large gas engines offer a premixed, homogeneous charge of fuel gas and air at ignition timing. Nevertheless, deficiencies in mixture formation due to the extreme boundary conditions can lead to inhomogeneities in the charge distribution at the spark plug, which makes reliable ignition of the mixture more difficult and can lead to cycle-to-cycle differences in combustion. This effect is more pronounced with a leaner mixture. Strictly speaking, a lean air-fuel mixture lowers the probability of the appearance of a combustible charge between the spark plug electrodes at ignition timing; dilution further reduces the ignitability of the mixture and the combustion speed, especially in the initial stage of combustion. In addition to high power density with very high efficiency, low nitric oxide ( $\text{NO}_x$ ) emissions are another main requirement for modern lean-burn gas engines. One possible strategy for reducing  $\text{NO}_x$  emissions in lean-burn engines is exhaust gas recirculation (EGR), which has proven to be a reliable method for reducing emissions from diesel engines. However, the application of EGR in large gas engines [4] not only leads to a dramatic increase in the complexity of hardware and control systems but also provides additional challenges for the ignition system [5]. Consequently, all these effects place much higher demands on the ignition system. The spark plug operates under more difficult boundary conditions and the use of conventional ignition systems may lead to increased cycle-to-cycle variations, incomplete combustion or even misfiring. Reliable ignition of the mixture is a challenge and may require new approaches to ignition systems [6].

An evaluation of new ignition systems must address the usability of the system with increasing charge dilution, robustness in the presence of very high ignition pressures and usability under highly inhomogeneous and transient ignition conditions

(both within a single engine combustion cycle and with regard to cycle-to-cycle variability). In the existing literature, the potential of an ignition concept is usually evaluated only for automotive applications, i.e. for relatively low pressures at the ignition timing. The question arises as to which alternative ignition concept can also be used in lean-burn engines. Furthermore, tolerance to high flow and turbulence at the ignition location is critical. This constantly growing list of requirements is completed by robustness in the face of difficult starting conditions and compatibility with an increasing number of fuel qualities and types. Additional concerns include the service life or maintenance interval of the ignition system of several thousand hours and low costs.

A large variety of possibilities exist for igniting a mixture in the combustion chamber; the requirements described for ignition in large gas engines present these ignition systems with various challenges [7]. In this paper, three selected ignition concepts – conventional spark ignition based on a modulated capacitive discharge ignition system (MCDI) [8], [9], laser ignition [10], [11] and diesel pilot ignition [12], [13] – are compared theoretically, numerically and experimentally under conditions that are as comparable as possible.

Today, electric spark ignition systems are the industry standard. These systems have been improved over more than a century and hence have reached a highly advanced level of development. Due to the large quantities produced, their cost is relatively cheap. However, spark ignition systems also have clear disadvantages especially when they are used with modern lean-burn combustion systems. For example, spark plug electrodes are exposed to wear especially in high pressure media, and the location of ignition is determined by the spark plug geometry and occurs near the cylinder wall. The performance of spark ignition ceases especially at lean burn conditions. As the possibilities of laser ignition have become more diverse and laser technology has become more powerful and cost-effective, interest in using laser ignition in gas engines as an alternative ignition system has increased in recent years. The advantages of laser ignition are basically twofold: extremely short yet energy-rich ignition and the introduction of energy at the most favorable point in the combustion chamber. In addition, laser ignition is hardly affected by stochastic influences that arise from the flow conditions in the cylinder. A further option for igniting a lean gas/air mixture in the prechamber or main combustion chamber is diesel pilot ignition. With an open chamber, the

diesel is injected into the combustion chamber and directly ignites the charge, while with a prechamber, the injected liquid fuel ignites the charge in the prechamber, which serves as an ignition amplifier, so that reliable ignition of the fuel gas-air mixture is achieved in the main combustion chamber.

This paper compares the three ignition concepts – spark ignition, laser ignition and diesel pilot injection – and evaluates their potentials. At first, theoretical considerations are introduced that discuss, inter alia, the available ignition energy of the three concepts. Next, highly sophisticated simulation models validated in prior research [14], [15] are presented that simulate the processes relevant to ignition, flame kernel development and combustion. Experimental investigations of all three ignition systems are conducted on a single-cylinder engine (SCE) at similar boundary conditions. In order to interpret the measurement results correctly, all operating points are recalculated with simulation models in 3D CFD simulation. The simulation results aid in understanding the effects in more detail and validating the measurement results. Finally, the potential of each of the alternative ignition systems is evaluated by comparing the results from measurement and simulation.

## 2 FUNDAMENTALS

Before the three ignition concepts can be compared, it is necessary to comprehend their fundamentals and their underlying processes. Only with a detailed understanding of the effects that occur is it possible to generate a fair comparison of the very different concepts and to plan and carry out the experimental and numerical investigations effectively. Since the fundamentals of these ignition concepts are very extensive, however, a detailed discussion would clearly go beyond the scope of this paper. Therefore, the following explanations only aim to provide a rough insight into the relevant mechanisms of the ignition concepts.

### 2.1 Spark ignition

This section briefly introduces the fundamentals of spark ignition, the process of electric gas discharge at a defined location between two electrodes of a spark plug. It explains the conditions and energy levels characteristic of the electronic ignition systems in spark ignited internal combustion engines and reveals how they relate to the electric side of the ignition system.

The following detailed analysis of the electric discharge provides an impression of the time scales at which electronic spark ignition takes

place. The different stages of electric discharge are illustrated in Figure 1, which consists of images of a spark plug electrode gap along with circuit diagrams that depict the main mode of energy transfer from the electric side of the ignition system. The circuit model of the ignition system presents a modulated capacitive discharge ignition system (MCDI), cf. [8], [9], an ignition system common in large gas engines. A high-speed camera with a frame rate of 120000 frames per second captured the spark plug gap images in a special arc test rig designed to facilitate an investigation of electric arc behavior under engine-like pressures and cross-flows at the spark plug under non-combustible conditions, cf. [16], [17]. The optical investigations in Figure 1 were conducted in an air atmosphere at 60 bar and 70°C.

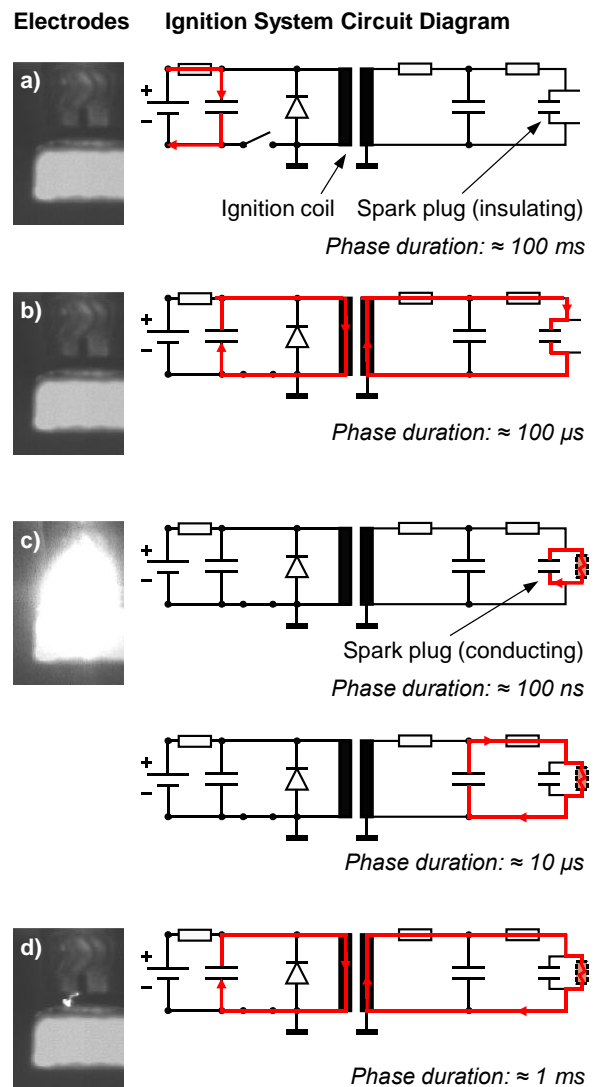


Figure 1. Spark discharge sequences in a capacitive ignition system [16]

Upon activation of the ignition system, the energy stored in a capacitor, Figure 1a), is transferred

from the primary side of the ignition system (in Figure 1, the left-hand side of the ignition coil, which acts as a transformer) to the secondary side, Figure 1b). As long as the gap between the spark plug electrodes is insulating, an initial rapid increase in the voltage across the electrode gap takes place until breakdown occurs, Figure 1c), cf. [16]

In the breakdown phase, streamers form between the electrodes, eventually creating a conductive channel. The only limit to the high electrical currents typical of this phase is the impedance of the secondary circuit of the ignition system. The energy stored in the capacitances on the secondary side is released on time scales of several hundred nanoseconds (spark plug capacitances) to microseconds (cable capacitances). This process is too rapid for pressure equilibration to take place; as a result, it occurs during the plasma expansion phase, in which a blast wave radiates out of the initial arc channel. The intense light emitted after breakdown is also visible in Figure 1c). At time scales on the order of several microseconds to one millisecond, the energy transfer from the primary capacitor to the ignition coil also encourages electric discharge, resulting in a distinct electric arc column typical of both the glow mode and arc mode, Figure 1d). In this last phase, the modulation of a switch on the primary side – usually an insulated gate bipolar transistor (IGBT) – shapes the spark power; this is the core principle of MCDI technology and allows the application of up to several hundred millijoules of energy for ignition. It should be remembered that the flow field at the spark plug has a few milliseconds during which it can interact with the electric arc column in the last phase of arc discharge. In this period, the electric arc raises the local gas temperature above the level favorable for the formation of an infant flame kernel, cf. [16]

The state of the electric arc strongly depends on two influencing factors: the prevailing thermodynamic conditions and the flow conditions at the spark plug. Strong cross-flows significantly influence the electric arc by means of arc stretching. Figure 2 provides an example of an elongated arc captured by a high-speed camera in the arc test rig, cf. [16], [17].



Figure 2. Electric arc stretching under cross-flow conditions

With the help of this test rig, it was found that electric arc stretching becomes greater when the flow velocity increases or when the system pressure increases at a defined flow velocity. In addition, greater arc stretching leads to larger cycle-to-cycle variations in arc length, cf. [16], [17]. Since the secondary voltage strongly depends on arc length, the cycle-to-cycle variations of the secondary voltage and thus of the secondary energy supplied to the flowing gas increase as well, cf. [16], [17], [18]. Under severe conditions with high charge motion and very lean gas-air mixtures such as those encountered in advanced large spark ignited gas engines, it is essential to understand these fundamental phenomena of electric arc behavior so that spark ignition technology can be best employed and the overall combustion system improved and optimized.

## 2.2 Laser ignition

A laser is a device that emits monochromatic coherent electromagnetic radiation [19]. It can be used in several different ways as an ignition system for combustion processes, cf. [20]. The present publication introduces in detail the effect of non-resonant breakdown, a laser ignition process in which a strong electric field is generated by a focused laser beam. At the focal point, free electrons are accelerated and obtain high energies. Collisions with gas molecules generate and accelerate secondary free electrons, leading to an avalanche process and the formation of plasma. The plasma is visible as a bright spot, cf. Figure 3; it creates heat and chemically active radicals which form a flame kernel that is able to ignite the combustible gas-air mixture, cf. [20].



Figure 3. Plasma generated by a laser pulse [20]

Even though the ignition of the gas-air mixture in an engine at a specific ignition point is similar to spark ignition, it should be noted that the position of the laser ignition point in the combustion chamber is defined with a large degree of freedom. Thus, it is possible to avoid quenching effects due to the proximity of the ignition point to the combustion chamber wall or the spark plug electrodes.

A laser ignition system typically produces highly intense laser pulses. A single pulse supplies an energy of several tens of millijoules for ignition of the gas-air mixture in the combustion chamber, cf. [20]. While the ignition voltage required to break down conventional electric sparks increases along with the prevailing pressure at spark timing (relevant for gas engines operated at high mean effective pressures), the minimum laser pulse energy for plasma generation decreases along with the pressure, cf. [20], [21]. Furthermore, stochastic flow effects only have minor impact on the initial plasma discharge as there is no such behavior as electric arc stretching due to the flow interaction that occurs in spark ignition systems.

### 2.3 Diesel pilot ignition

With diesel pilot ignition, a small amount of diesel fuel is injected into the combustion chamber as the ignition source, cf. [22], [23]. The injected diesel mass normally accounts for approximately one to some percent of the total energy input to the cylinder, enabling the combustible gas-air mixture to ignite at multiple locations and with a large initial ignition volume, cf. [22], [23]. Similar to diesel engines, the injected pilot diesel fuel relies on a compression ignition process in which the ignition delay time plays an important role. This time is defined as the time between the start of injection and the start of combustion, cf. [24], [25]. During the ignition delay time, chain branching reactions take place that result in the formation of radicals, but the temperature of the system does not change noticeably [26]. Due to knocking, the compression ratio of diesel ignited gas engines is significantly lower than that of mono-fuel diesel

engines, cf. [27], [28], [29], [30]. Hence, a considerably lower pressure and temperature level prevail in the combustion chamber at the end of compression under otherwise identical conditions at intake valve closing. Since the ignition delay time strongly depends on temperature, cf. [26], it is generally longer in the diesel ignited gas engine than in the diesel engine, cf. [31]. Due to these long ignition delay times, early pilot injection timings well before top dead center are required, which in turn leads to even lower initial temperatures in the combustion chamber and to a further prolonged ignition delay.

Figure 4 presents the influence of temperature and pressure on ignition delay time. The curves represent the calculated ignition delay times as a function of the initial temperature at selected pressures of a stoichiometric mixture of N-heptane, the diesel reference fuel, and air. The ignition delay time sharply decreases at higher initial temperatures. A so-called "negative temperature coefficient" (NTC) typical of long-chain alkanes is clearly visible. The NTC indicates that in a certain range (NTC regime), the ignition delay time increases as the initial temperature goes up [25]. Figure 4 also shows that the influence of pressure on the ignition delay is much more pronounced in the NTC range than in the adjacent high and low temperature ranges. On the basis of engine measurement data, it was determined that the low temperature and NTC ranges are important in the ignition process due to the comparatively low compression ratio of diesel ignited gas engines.

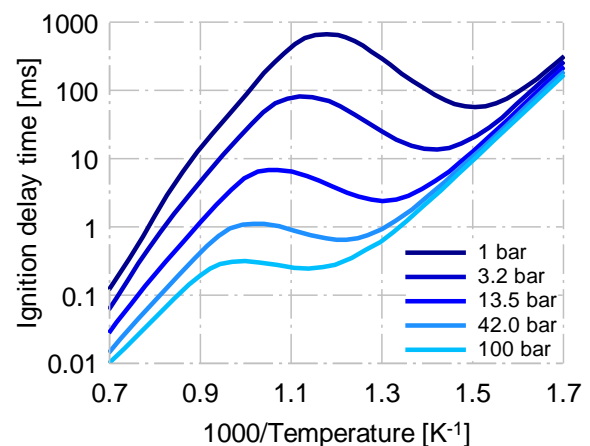


Figure 4. Influence of initial temperature and pressure on ignition delay time [32]

Another influencing factor for the self-ignition of diesel-air mixtures is the mixture quality. Ciezki and Adomeit [33] as well as Pfahl et al. [34] have shown in shock tube experiments with the diesel reference fuels N-heptane and N-decane that the

ignition delay time of a diesel-air mixture becomes lower as excess air ratio decreases. An example of this behavior is shown in Figure 5 at a constant pressure of about 40 bar.

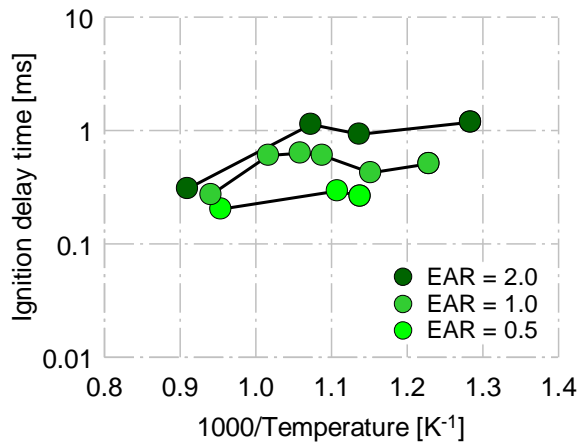


Figure 5. Influence of initial temperature and excess air ratio on ignition delay time [33]

Due to the comparatively long ignition delay time of diesel ignited gas engines, the diesel fuel may be highly homogenized with the background mixture during the ignition delay time, especially with small injected diesel amounts and early injection timings. This in turn may lead to an increase in the local excess air ratio in the area of the injected diesel fuel, resulting in a longer ignition delay time. Thus, the ignition delay time is affected not only by the temperature and pressure in the combustion chamber at the start of injection but also by the process of mixture formation and the interaction between the diesel fuel and the background mixture.

The parameters temperature, pressure and local excess air ratio in the area of the pilot fuel jet do not yet reflect the influence of the fuel gas in the homogeneous background mixture on the ignition delay time. The inhibitory effect of methane in diesel ignited gas engines is well researched. Fundamental investigations of Pischinger [35] and Schlatter et al. [36] illustrate that under otherwise identical boundary conditions, the ignition delay time of diesel injection into a methane-air mixture is significantly higher than that of diesel injection into pure air. In addition, the ignition delay time increases as the excess air ratio of the methane-air mixture decreases. Figure 6 shows the influence of the equivalence ratio of the background mixture on ignition delay time. The investigation was carried out under engine-like conditions and illustrates the inhibitory effect of methane. At an equivalence ratio of 0.65 (corresponding to an excess air ratio of approx.

1.5), the ignition delay is nearly twice as long as at an equivalence ratio of 0 (pure air).

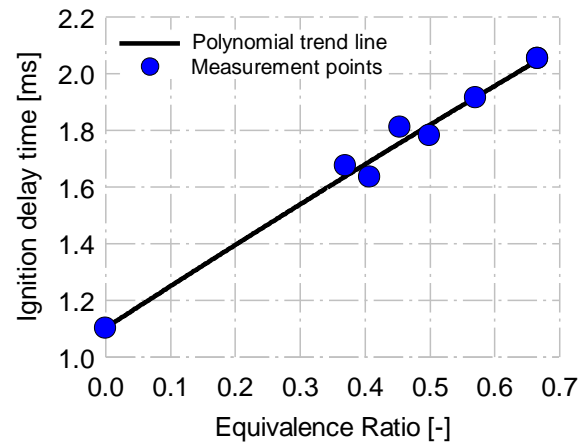


Figure 6. Influence of equivalence ratio of methane-air background mixture on ignition delay time [36]

In summary, the ignition delay in diesel ignited gas engines provides time for mixture preparation. Likewise, ignition delay time is influenced by mixture preparation. Pressure and temperature at the start of injection have a significant influence on the ignition delay time, but it must be remembered that these parameters do not remain constant after the start of injection due to the ongoing compression process. The ignition process, therefore, is highly transient. The excess air ratio of the homogeneous gas-air background mixture also influences the ignition delay time since methane inhibits ignition. Based on a fundamental understanding of these effects, a target-oriented improvement of the ignition and the combustion process can be strived for.

### 3 METHODOLOGY

This section discusses the methodology used to compare the three ignition concepts whose fundamentals were presented in the previous chapter. First, experimental investigations are carried out on an SCE, whereby a particular emphasis is laid on investigating each ignition concept under boundary conditions that are as comparable as possible. The results obtained from the experimental investigations are then examined in detail using numerical CFD simulation methods in order to better understand the relevant effects of the ignition system on the ignition and combustion process. The following section explains the setup for the experimental investigations and the numerical setup for the simulations.

### 3.1 Setup for experimental investigations

The experimental investigations were carried out on an SCE that consists of a base frame housing the engine's power unit and a specially designed crankshaft. Furthermore, the engine has a first and second order mass balancing system, an oversized flywheel and a four-quadrant dynamometer to motor and brake the engine. The charge air is supplied by a screw-type compressor. The air is cooled for dehydration and then heated to the desired temperature level. The water content of the cylinder charge is adjusted via steam admixed to the charge air. The fuel gas is mixed with the charge air on the high-pressure side using a Venturi mixer. To simulate the exhaust back pressure of a multi-cylinder engine (MCE), a throttle flap is placed in the exhaust piping. The pressure drop is calculated with the turbocharger equation. The SCE test bed is equipped with an exhaust gas analysis device that determines the concentrations of the most important components, namely CO<sub>2</sub>, O<sub>2</sub>, CO, THC, CH<sub>4</sub> and NO<sub>x</sub>. The cylinder head of the engine is fitted with fast pressure transducers that indicate the pressure trace in the main combustion chamber and prechamber as well as the intake and exhaust ducts.

The design of the single-cylinder research engine is based on a high-speed gas engine for power generation. The power unit configuration was taken from pre-series parts of the reference multi-cylinder engine; for technical data cf. Table 1. The piston setup (flat shape and compression ratio) and camshaft (early Miller valve timing) were the same throughout the investigations. Furthermore, the following boundary conditions for the tests were kept constant to the greatest extent possible: boost pressure, exhaust back pressure, excess air ratio, intake manifold temperature and water content of the fresh cylinder charge.

Table 1. Main technical data of SCE

	SCE
Displacement [dm <sup>3</sup> ]	~ 6
Nominal BMEP [bar]	22
Rated speed [rpm]	1500

The experimental investigations were divided into two groups. Table 2 summarizes the investigated ignition concepts. First, different ignition concepts for a prechamber combustion concept were compared. The reference engine for the investigations uses a gas-scavenged prechamber with an MCDI system and a J-gap spark plug. This configuration is hereafter referred to as the spark ignition concept. The identical prechamber

concept (same scavenging gas quantity and prechamber geometry) was also operated with a Q-switched, pulsed Nd:YAG laser ignition system. The laser employed a wavelength of 1064 nm. The focal point of the laser was set to the same position as the electrode gap of the spark ignition, thereby avoiding cross influences of the initial point of inflammation on the benchmark. Setting the focal point of the laser to a different position might result in advantages or drawbacks, but was not part of the presented investigations. This configuration is referred to as the laser ignition concept. Furthermore, the prechamber was also operated with a diesel jet; this configuration is referred to as the diesel MicroPilot concept. The amount of diesel fuel introduced (energetic share related to the total fuel energy supplied to the engine) corresponded to the amount of prechamber scavenging gas for spark ignition and laser ignition. To this end, an automotive common rail diesel injector was equipped with a specially designed nozzle configuration and integrated into the cylinder head. The nozzle was designed with four spray holes and a nominal nozzle flow of 165 ml/30s @ 100 bar. The rail pressure was set to 1600 bar.

The second group of investigations focused on the ignition of the charge in the main combustion chamber. The gas-scavenged prechamber with spark ignition again served as the baseline. Regarded as the ignition source for the charge in the main combustion chamber, it was compared with an operation with diesel jet ignition into the main combustion chamber. The nozzle configuration (number of spray holes, geometry and flow rate) was identical to the one in the diesel MicroPilot configuration. This nozzle was chosen in order to enable full lift of the injector needle with very low injected fuel quantities, because it represented the minimum flow rate available. This should guarantee a low cycle-to-cycle variation of the injection events.

Table 2. Investigated ignition concepts

Focus of investigations	Ignition concept
Prechamber	Spark ignition
	Laser ignition
	Diesel MicroPilot
Main chamber	PC w/ spark ignition
	Diesel pilot

## 3.2 Numerical modeling approaches

### 3.2.1 General numerical setup

The simulation setups were also kept as similar as possible in order to ensure consistency in the simulation of all the experimental setups. Table 3 provides an overview of the modeling approaches that are used in each of the different simulations and includes the average cell size of the meshes. Refinements were made in relevant areas, especially in the region where ignition is expected to occur, depending on the ignition system to be simulated.

Table 3. Modeling approaches for all simulations

Modeling approaches	
Turbulence	k- $\zeta$ -f model [37]
Thermodynamics	Ideal gas law
Combustion	ECFM approach for laser and spark ignition [38]
	ECFM-3Z approach for diesel pilot in the prechamber [39], [40]
Numerical settings	
Pressure-velocity coupling	SIMPLE algorithm [41]
Average cell size	1.5 mm with refinements to inlet/outlet ports and pre-chamber as well as ignition region

The boundary conditions were obtained from the experimental investigations on the engine test bed and were post-processed with a 0D engine cycle calculation program to provide the thermodynamic starting conditions for CFD calculations.

### 3.2.2 Combustion and ignition modeling approaches

The modeling approaches differ in response to the variety of ignition systems. Combustion was modeled using the Extended Coherent Flame Model (ECFM) approach with modifications based on the ignition system.

The spherical spark ignition model was used for the spark ignited prechamber. In this model, a spark position is defined in the simulation domain and within a specified radius referred to as the ignition radius, all finite volume cells are treated as if ignition has occurred. To start the flame front propagation, a constant initial flame surface density  $\Sigma_{ini}$  is defined for each cell for the specified duration of ignition. Figure 7 depicts this ignition model.

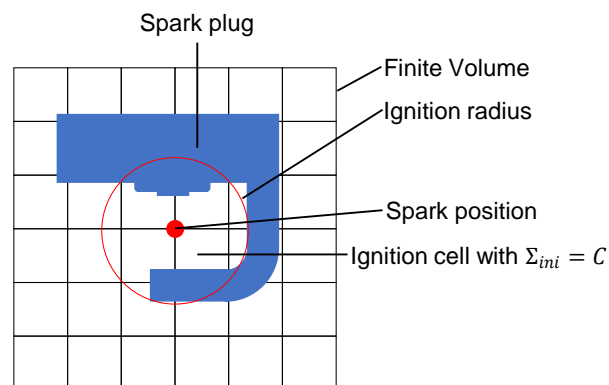


Figure 7: Schematic of spherical ignition model used for the spark ignited prechamber and laser ignited prechamber

To be consistent with the spark ignition modeling, the spherical ignition model was also selected to simulate laser ignition; however, the electrode brackets of the spark plug were removed from the geometry. The ignition radius of the flame surface used for the subsequent combustion was estimated with the model in [14] (reformulated for a spherical plasma kernel), which relies on the well-known similarity solution for strong blast waves from [42] and [43]. Assuming the problem is spherical and the breakdown energy is supplied quasi-instantaneously as a point source, the extent of the hot plasma kernel and the time for pressure equalization with the surrounding area can be determined from the known energy input of the laser pulse by exploiting the properties of radially expanding blast waves. This control volume is treated as an open system, and a simple energy balance using detailed constitutive relations for air plasma in local thermodynamic equilibrium yields a relation for the mean kernel temperature and mean plasma radius.

The ECFM model with the 3 zones approach (ECFM-3Z) [39] was applied to the diesel pilot concept and adopted for diesel/natural gas combustion in large gas engines based on the works of [15]. The standard WAVE model was used for diesel pilot injection with calibration and input data according to [40]. The rate of injection was determined by flow rate measurements and could therefore be prescribed in the model. The ignition delay was calculated using specific dual fuel tables as described in [15] and [44]. The subsequent initialization of the flame surface density after ignition was described according to the following idea. After a specific computational cell has been ignited (which is equivalent to having passed the ignition delay time), the ignited cell must obtain an initial value for the flame surface density to start the flame front propagation. Using the gradient of the progress variable formed by the consumption of fuel during

autoignition, the flame contour can be “reconstructed.” This idea is depicted in Figure 8.

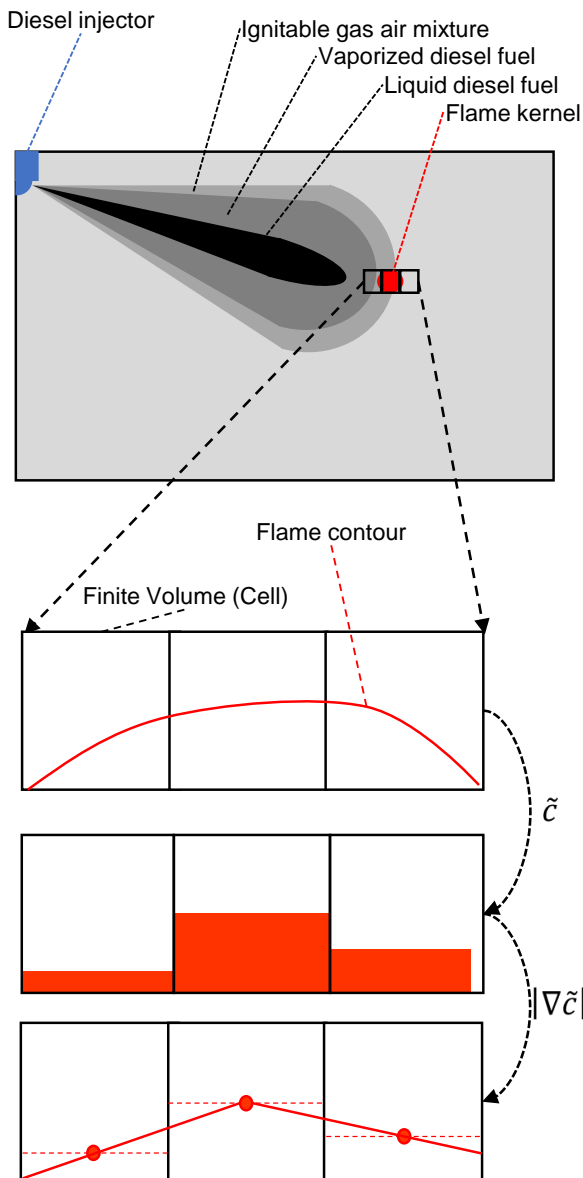


Figure 8: Schematic of diesel pilot ignition model for the diesel ignited prechamber and diesel ignited main chamber

The initial flame surface density is modeled with the following equation:

$$\Sigma_{ini} = C * |\nabla \tilde{c}| * \left( 1 + \frac{\sqrt{k}}{\bar{u}} \right) \quad (1)$$

C being a calibration constant,  $\tilde{c}$  the Favre averaged progress variable,  $k$  the turbulent kinetic energy and  $\bar{u}$  the mean velocity. After the flame kernel is initialized, flame propagation starts. Propagation through a potentially dual fuel mixture (due to the diesel mixing with natural gas and air before ignition) is accounted for again using

specific dual fuel tables [44] for the laminar flame speed in the ECFM-3Z model approach.

#### 4 DISCUSSION OF RESULTS

The boundary conditions for the comparison of spark ignition, laser ignition and diesel MicroPilot ignition in the prechamber were first derived for the baseline configuration (spark ignition). The engine load was set to 22 bar brake mean effective pressure (BMEP) (equivalent to the MCE given the difference in friction behavior between the MCE and SCE). The goal was to achieve a  $\text{NO}_x$  emission level of  $500 \text{ mg/m}^3 \text{ Norm @ 5\% O}_2$ , the TA Luft emission limit, while keeping the effective ignition time constant during all investigations.

Figure 9 compares the results of the investigations with the prechamber. The spark ignition result values are set as the baseline value (100%) and the relative changes in the functional values for laser ignition and diesel MicroPilot are displayed. A distinct difference is found with regard to the maximum pressure difference between prechamber and main combustion chamber. Whereas the excess pressure with laser ignition is only slightly lower than with spark ignition, the operating point with diesel MicroPilot shows a relative increase of more than 150%. Note that the fuel energy introduced into the prechamber by the diesel spray was set in accordance with the amount of gas fed into the scavenged prechamber. All investigated concepts have almost identical efficiency in the high-pressure (HP) cycle with a slight advantage for diesel MicroPilot ignition. This advantage mainly results from the lower losses due to the real combustion process (Real Comb.), i.e. the difference between the efficiencies of the adiabatic high-pressure processes with isochore combustion and real combustion [26]. This lower loss is due to the earlier combustion phasing that can be partly attributed to the high maximum excess pressure in the prechamber. Efficiency losses due to incomplete combustion (Incompl. Comb.) are slightly lower for both laser ignition and MicroPilot ignition. Furthermore, the delay between the diesel injection start of current and start of injection was overcompensated for in comparison to the spark timing. Figure 10 graphs the normalized rates of heat release of the three selected operating points. While the combustion behavior of spark ignition and laser ignition is nearly identical, the advanced combustion phasing of diesel MicroPilot is clearly visible. The initial steep rise in rate of heat release induced by the flame jets exiting the prechamber, however, is also very similar in all three investigated variants.

The pressure difference in the prechamber is also apparent in the 3D CFD results (cf. Figure 12).

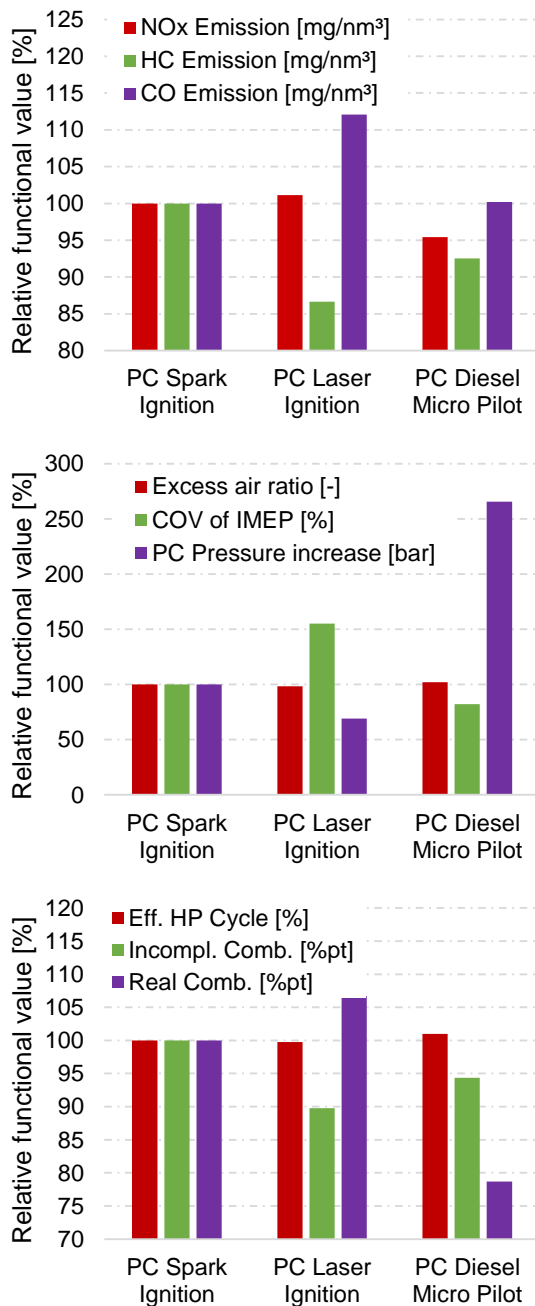


Figure 9. SCE results: PC ignition concepts

Figure 11 shows the pressure trace from measurement and 3D CFD simulations. All pressure traces show sufficiently good agreement with the 3D CFD simulation results, ensuring the validity of further analysis of the 3D results. Differences in simulation and measurement can be seen for the combustion in the main chamber in the spark ignition case. As the focus of the CFD results is on the prechamber this difference is not considered in the further discussion. Due to the same ignition model approach being used for

spark and laser ignition one can see no significant difference in the CFD results in the initial stage of prechamber pressure increase for spark and laser ignition.

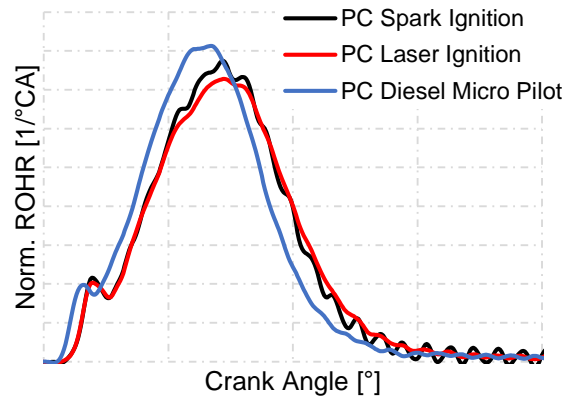


Figure 10. Rate of heat release of selected PC ignition concept operating points

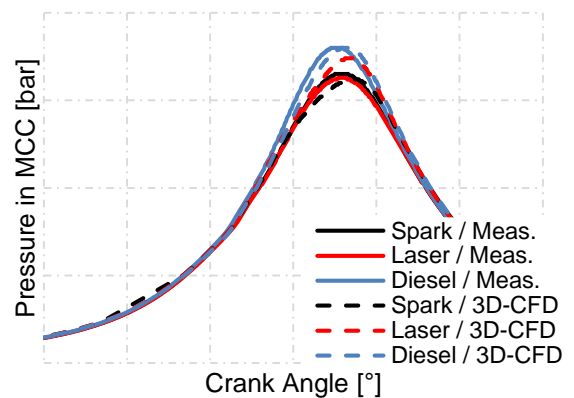


Figure 11: Comparison of pressure traces of selected prechamber concepts

A comparison of the pressures in the prechambers aimed to confirm the strong pressure increase in the diesel ignited prechamber, see Figure 12.

The diesel ignited prechamber shows a steeper gradient of the pressure increase and also a higher absolute value in terms of prechamber peak pressure. This confirms the measurement data regarding the rate of heat release shown in Figure 10. However, the absolute increase compared to the spark ignited prechamber could not be reproduced.

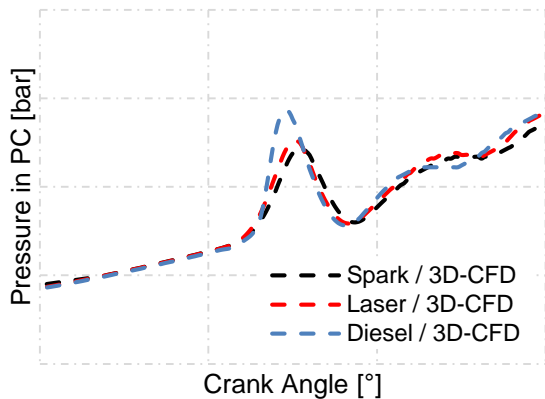


Figure 12: 3D CFD simulation results of the prechamber pressures of selected ignition concepts

To further interpret the measurement results, Figure 13 presents the prechamber pressure traces and cut planes of the 3D CFD simulations at selected crank angles. The cut planes represent spark ignition on the top (black frames), laser ignition in the middle (red frames) and the diesel ignition on the bottom (blue frames). These cut views show the progress variable in the simulation. The status of the gas ranges from fully burned (red) to unburned (blue). The progress variable is therefore a reasonable scalar for identifying the current location of the flame front.

The left-hand images in Figure 13 show the transition of the flame torches from the prechamber to the main chamber. As already seen in the measured ROHR and confirmed by the prechamber pressure trace from the 3D CFD simulation, the flame in the prechamber burns faster with diesel ignition, as indicated by the flame torches exiting the prechamber bores. In the center images in Figure 13 the flame has exited the prechamber bores in all three cases. It can be seen that there is a noticeable difference in penetration between the three cases. However, the combustion characteristics that ensue after the charge exits the prechamber bores are rather similar in all three cases (cf. right-hand images in Figure 13), hence not significantly influenced by this difference. This behavior may be caused by the supercritical flow conditions at the exit of the prechamber bores; in particular in case of the diesel MicroPilot.

The next step of the investigations compares the ignition concepts and their direct effect on the main combustion chamber. This comparison includes a gas-scavenged prechamber with spark ignition and diesel pilot ignition. The amount of fuel injected was increased by 50% of the amount used in the experiments with diesel MicroPilot; the

nozzle configuration remained the same. A variation in the start of current yielded a relatively large range of functional values. Two operating points were selected for the direct comparison with the prechamber and spark ignition, whereby the first operating point (Op.Pt. 1) has the same combustion phasing as the prechamber operating point. In the other case, the NO<sub>x</sub> emission level achieved with the second operating point (Op.Pt. 2) is the same (TA Luft) as with the prechamber operating point, cf. Figure 14. The start of current of Op.Pt. 1 is five degrees later than that of Op.Pt. 2.

One result of this investigation of boundary conditions is that the NO<sub>x</sub> emissions of Op.Pt. 1 are significantly higher. Furthermore, emissions of unburned hydrocarbons and carbon monoxide also increase. However, the levels of HC and CO emissions of Op.Pt. 2 are even higher: 400% and more than 350%, respectively. The excess air ratio of the operating points in the diesel pilot tests also reached the same level as in the prechamber tests. The combustion stability is significantly lower; Op.Pt. 1 is just at the stability limit, while Op.Pt. 2 is well beyond this limit. The high HC and CO emissions cause a significant increase in losses due to incomplete combustion of 150% and 300%, respectively. An additional loss is due to the late combustion phasing of Op.Pt. 2. In total, the efficiency of the high-pressure loop is reduced by 4% and 8%, respectively.

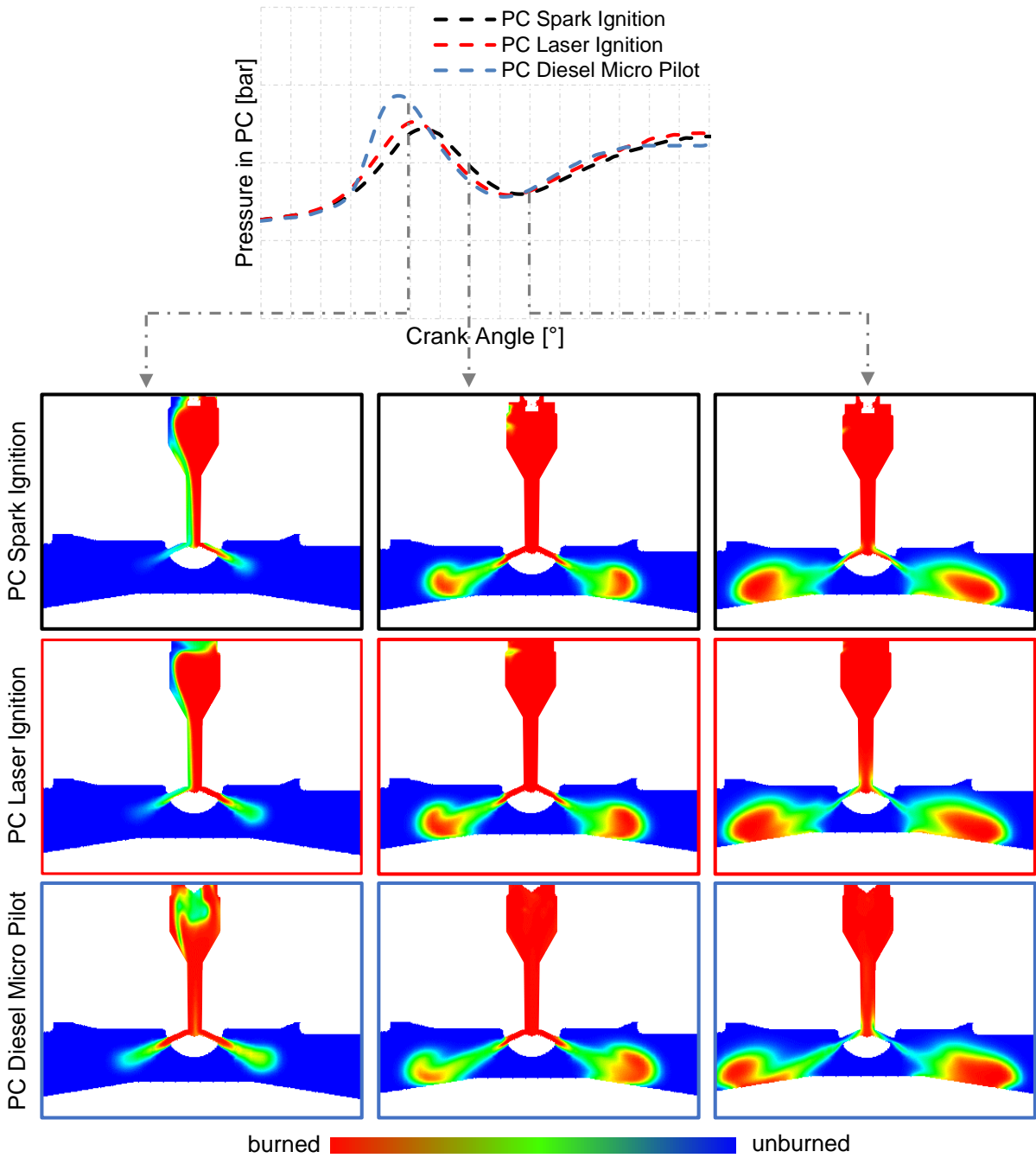


Figure 13. 3D CFD cut planes showing the progress variable for selected prechamber concepts – Flame torches exiting the prechamber bores

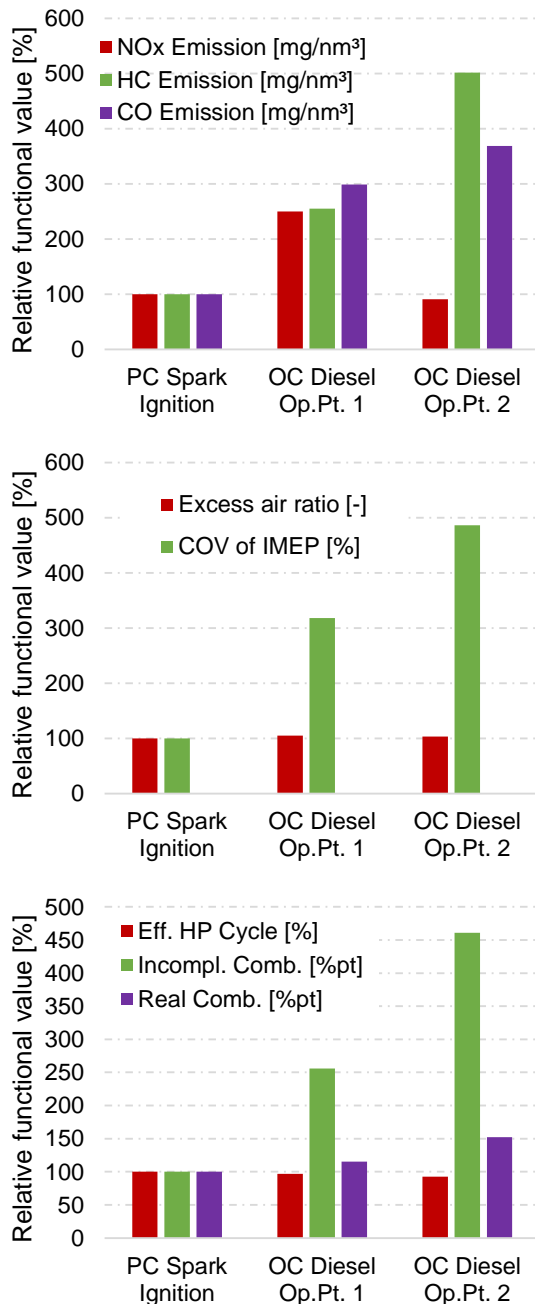


Figure 14. SCE results: open chamber concepts

The rates of heat release indicate that Op.Pt. 1 has a very intensive and rapid increase in fuel conversion (Figure 15). However, lower peak conversions are recorded than in the prechamber test. In addition, slower burnout is visible. The fuel conversion of Op.Pt. 2 increases only slightly in the beginning, and the rise in the combustion process up to the peak conversion is flatter and thus slower than in the other two cases. Burnout occurs very slowly.

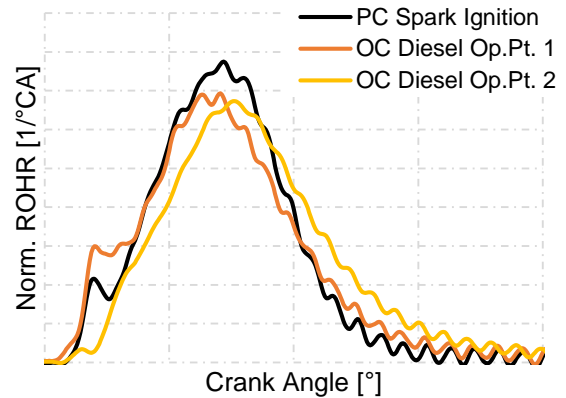


Figure 15. ROHR comparison, open chamber ignition concepts

Once again it is worth noting that the combustion phasing of Op.Pt. 2 is later than that of Op.Pt. 1 despite the earlier injection timing. This phenomenon is explained by pronounced homogenization (“overmixing”) of the injected diesel fuel with the lean background mixture. As a consequence, ignition delay is significantly increased and the initial rate of heat release is reduced, cf. [12], [13], [23].

## 5 SUMMARY AND CONCLUSIONS

This paper compared the potentials of three different ignition concepts (spark ignition, laser ignition and diesel pilot ignition) when applied to a large lean-burn gas engine. A short summary of the most important fundamentals provided insight into the mechanisms underlying the different ignition systems. An understanding of these basic characteristics facilitated the investigations. The required backgrounds of the simulation methods were explained. The special feature of the investigation methodology was that all relevant boundary conditions were set so that they could be compared as easily as possible, allowing consistent statements to be made based on both the experimental and the numerical investigations.

The results of the experimental and numerical investigations and simulations were evaluated and discussed. Although the potential of the alternative prechamber ignition systems (laser ignition and diesel MicroPilot) to ensure a robust ignition process is theoretically available, neither the experimental nor the numerical investigations were able to confirm this potential. The results also show that compared to a prechamber spark ignition concept, using a diesel pilot injection in an open chamber configuration is not a preferable option.

As the investigations have illustrated, diesel MicroPilot injection in the prechamber could have slight advantages in terms of achievable efficiency, but the use of this system goes hand in hand with an increase in system complexity. For all investigated diesel pilot injection configurations, a second fuel supply is required, although pure diesel operation is not possible anyway. Very high temperatures at the injection nozzle in the prechamber pose further challenges that must be overcome when using this system. The configurations with diesel injection are also expected to have disadvantages with regard to the energy consumption of the systems. In the case of laser ignition, the system costs must also be taken into account; here it is questionable whether the achievable improvement potential of the system justifies the increased cost requirements.

It can be stated that a prerequisite for this study was to ensure that the boundary conditions for the investigated systems were as comparable as possible, which on the one hand resulted in a limited number of measurement data sets, and on the other hand may have led to the fact that the examined configurations probably do not represent the optimum. Individual optimization of each system can result in better performance. In order to obtain a more general statement on this topic it is absolutely necessary to have a larger number of measurement data available; further variations, e.g., in the case of laser ignition the variation of the ignition location, or in the case of pilot injection the variation of the nozzle parameters, are also absolutely necessary in order to consolidate the statements.

In summary, given the advantages and disadvantages of these ignition systems, the economic and legal boundary conditions and the comparative investigations described in this paper, the prechamber with spark ignition can still be regarded as the most promising ignition system for the large gas engines of the future. Conventional spark ignition embodies a system that is cost-effective and easy to maintain, requires no secondary fuel supply and requires no additional energy for ancillary systems.

## 6 ACKNOWLEDGEMENTS

The authors would like to acknowledge the financial support of the "COMET - Competence Centres for Excellent Technologies Programme" of the Austrian Federal Ministry for Transport, Innovation and Technology (BMVIT), the Austrian Federal Ministry of Science, Research and Economy (BMWFW) and the Provinces of Styria, Tyrol and Vienna for the K1-Centre LEC EvoLET. The COMET Programme is managed by the Austrian Research Promotion Agency (FFG).

## 7 DEFINITIONS, ACRONYMS, ABBREVIATIONS

BMEP	Brake mean effective pressure
CFD	Computational Fluid Dynamics
CH <sub>4</sub>	Methane
CO	Carbon monoxide
CO <sub>2</sub>	Carbon dioxide
Comb.	Combustion
COV	Coefficient of variation
EAR	Excess air ratio
ECFM	Extended Coherent Flame Model
ECFM-3Z	Extended Coherent Flame Model with 3 Zones
Eff.	Efficiency
EGR	Exhaust gas recirculation
HC	Hydrocarbon
HP	High pressure
IGBT	Insulated gate bipolar transistor
IMEP	Indicated mean effective pressure
Incompl.	Incomplete
MCC	Main combustion chamber
MCDI	Modulated capacitive discharge ignition system
MCE	Multi-cylinder engine
Nd:YAG	Neodymium-doped yttrium aluminum garnet
NO <sub>x</sub>	Nitrogen oxides
NTC	Negative temperature coefficient
O <sub>2</sub>	Oxygen
OC	Open chamber
Op.Pt.	Operating point
PC	Prechamber
ROHR	Rate of heat release
SCE	Single cylinder engine
SIMPLE	Semi Implicit Momentum and Pressure Linked Equations
THC	Total hydrocarbons

## 8 REFERENCES AND BIBLIOGRAPHY

[1] Verdolini, E., Vona, F., Popp, D. 2016. Bridging the Gap: Do Fast Reacting Fossil Technologies Facilitate Renewable Energy Diffusion?, *NBER - National Bureau of Economic Research*, Working paper 22454, Cambridge, MA, USA.

- [2] Warnecke, W., Karanikas, J., Levell, B., Mesters, C., Schreckenber, J., Adolf, J. 2013. Gas – A Bridging Technology for Future Mobility? *34<sup>th</sup> International Vienna Motor Symposium*, Vienna, Austria.
- [3] Wimmer, A., Pirker, G., Engelmayer, M., Schnessl, E. 2011. Gas Engine Versus Diesel Engine: A Comparison of Efficiency, *MTZ Industrial*, Volume 1, November 2011, pp. 2-6.
- [4] Wimmer, A., Pirker, G., Zelenka, J., Chmela, F., Zurlo, J., Trapp, C. 2013. The Potential of Exhaust Gas Recirculation in Large Gas Engines, *CIMAC Congress 2013*, Paper No. 271, Shanghai, China.
- [5] Zelenka, J. 2015. Zum Einfluss der Abgasrückführung auf die Verbrennung in Großgasmotoren, Dissertation, Graz University of Technology, Graz, Austria.
- [6] Meyer, G., Gschirr, A., Lindner-Silvester, T., Stadlbauer, K. 2013. Recent Advances in Modeling Modulated Capacitive High-Energy Ignition Systems and Application of the Findings in a New Generation of Ignition System, *14<sup>th</sup> Conference The Working Process of the Internal Combustion Engine*, Graz, Austria.
- [7] Graf, J., Lauer, T. 2012. Identifizierung technisch und wirtschaftlich umsetzbarer Zündsysteme und Demonstration der grundsätzlichen Potenziale an unterschiedlichen Ottomotorkonzepten, Abschlussbericht, *FVV Heft 959-2012*, Frankfurt am Main, Germany.
- [8] Lepley, J., Brooks K., Bell D. 2010. A New Technology Electronic Ignition Which Eliminates the Limitations of Traditional Ignition Systems, *CIMAC Congress 2010*, Paper No. 173, Bergen, Norway.
- [9] Meyer, G., Salbrechter S., Titz A., Wimmer A. 2017. Assessment of Electric ARC Models Used in Recent Spark Ignition Models, *8<sup>th</sup> European Combustion Meeting*, Dubrovnik, Croatia, pp. 644–648.
- [10] Herdin, G., Klausner, J., Winter, E., Weinrotter J. G., Iskra, K. 2005. Laserzündung für Gasmotoren – 6 Jahre Erfahrungen, *4<sup>th</sup> Dessau Gas Engine Conference*, Dessau, Germany, pp. 44ff.
- [11] Brüggemann, D., Hüttl, C. 2009. Stand der Entwicklung bei Laserzündung, *Motortechnische Zeitschrift*, Volume 70, 03/2009, pp. 228-231.
- [12] Redtenbacher, C., Kiesling, C., Malin, M., Wimmer, A., Pastor, J.V., Pinotti, M. 2016. Potential and Limitations of Dual Fuel Operation of High Speed Large Engines, *ASME 2016 Internal Combustion Engine Fall Technical Conference, ICEF2016*, ICEF2016-9359, Greenville, SC, USA.
- [13] Redtenbacher, C., Kiesling, C., Malin, M., Wimmer, A., Pastor, J.V., Pinotti, M. 2018. Potential and Limitations of Dual Fuel Operation of High Speed Large Engines, *Journal of Energy Resources Technology*, Vol. 140, Issue No. 3.
- [14] Meyer, G., Wimmer, A. 2018. A thermodynamic model for the plasma kernel volume and temperature resulting from spark discharge at high pressures, *Journal of Thermal Analysis and Calorimetry*, Volume 133, pp. 1195-1205.
- [15] Eder, L., Ban, M., Pirker, G., Vujanovic, M., Priesching, P., Wimmer, A. 2018. Development and Validation of 3D-CFD Injection and Combustion Models for Dual Fuel Combustion in Diesel Ignited Large Gas Engines, *Energies*, Volume 11, Issue No. 643.
- [16] Titz, A., Meyer, G., Kiesling, C., Pirker, G., Salbrechter, S., Wimmer, A. 2019. Design of a Test Rig for Fundamental Investigations of Spark Characteristics. *International Journal of Engine Research*, in press, available on the internet at <https://doi.org/10.1177/1468087419828943>.
- [17] Titz, A., Meyer, G., Kiesling, C., Pirker, G., Salbrechter, S., Wimmer, A. 2018. Test Rig for Fundamental Investigations of Ignition Systems Characteristics under Severe Flow Conditions, *Ignition Systems for Gasoline Engines, 4<sup>th</sup> International Conference*, Berlin, Germany, pp. 75-90.
- [18] Pirker, G., Wimmer, A., Meyer, G., Kiesling, C., Nickl, A., Titz, A. 2018. Diagnostic Methods for Investigating the Ignition Process in Large Gas Engines, *13. Internationales AVL Powertrain Diagnostik Symposium*, Baden Baden, Germany.
- [19] Sigrist, M. W. 2018. *Laser: Theorie, Typen und Anwendungen*, 8<sup>th</sup> ed., Springer Spektrum, Berlin, Germany, p. 9.
- [20] Puhl, M. 2007. *Corona and Laser Ignition in Internal Combustion Engines*, Diploma Thesis, Vienna University of Technology, Vienna, Austria.
- [21] Kopecek, H., Charareh, S., Lackner, M., Forsich, Ch., Winter, F., Klausner, J., Herdin, G. and Wintner, E. 2003. Laser Ignition of Methane-Air Mixtures at High Pressures and Diagnostics. *ICES03 2003 Spring Technical Conference of the ASME Internal Combustion Engine Division*, ICES2003-614, Salzburg, Austria.
- [22] Redtenbacher, C., Kiesling, C., Wimmer, A., Sprenger, F., Fasching, P., Eichseder, H. 2016. Dual Fuel Combustion – A Promising Concept for Small to Large Engines? *37<sup>th</sup> International Vienna Motor Symposium*, Vienna, Austria.

- [23] Kiesling, C. 2017. *Analyse von Diesel-Gas Dual Fuel Brennverfahren für schnelllaufende Großmotoren*, Dissertation, Graz University of Technology, Graz, Austria.
- [24] Mollenhauer, K., Tschöke, H. (eds.) 2007. *Handbuch Dieselmotoren*, 3<sup>rd</sup> ed., Springer, Berlin, Germany, pp. 74f.
- [25] van Basshuysen, R., Schäfer, F. (eds.) 2015. *Handbuch Verbrennungsmotor; Grundlagen, Komponenten, Systeme, Perspektiven*, 7<sup>th</sup> ed., Springer Vieweg, Wiesbaden, Germany, p. 628.
- [26] Pischinger, R., Klell, M., Sams, T. 2009. *Thermodynamik der Verbrennungskraftmaschine*, 3<sup>rd</sup> ed., Springer, Vienna, Austria, pp. 102f.
- [27] Bergmann, D., Ghetti, S., Geiger, J., Virnich, L., Methfessel, P., Marten, C. 2017. VCR – Key technology for high efficient Dual-Fuel-Engines, *Variable Compression Ratio, International FEV Conference*, Garmisch-Partenkirchen, Germany.
- [28] Böckhoff, N., Hanenkamp, A. 2007. Der 51/60DF von MAN Diesel SE - Der leistungsstärkste 4-Takt Dual Fuel Motor, *5th Dessau Gas Engine Conference*, Dessau, Germany.
- [29] Kammerdiener, T., Schlick, H., Schönbacher, M., Zallinger, M., Hirschl, G. 2015. Konzeptuntersuchungen für einen Dual Fuel Motor basierend auf Versuchen an einem schnelllaufenden Einzylindermotor, *9th Dessau Gas Engine Conference*, WTZ Roßlau gGmbH Dessau, Germany.
- [30] Pischinger, S. 2016. Wie Gesetzgebungen und Kundenanforderungen Innovationen Beeinflussen, *4. Rostocker Großmotorentagung*, Harndorf H., Rostock, Germany.
- [31] Krenn, M., Pirker, G., Wimmer, A., Djuranec, S., Meier, M.C., Waldenmaier, U., Zhu, J. 2014. Methodology for Analysis and Simulation of Dual Fuel Combustion in Large Engines, *THIESEL 2014 Conference on Thermo- and Fluid Dynamic Processes in Direct Injection Engines*, Valencia, Spain.
- [32] Peters, N., Paczko, G., Seiser, R., Seshardi, K. 2002. Temperature Cross-Over an Non-Thermal Runaway at Two-Stage Ignition of N-Heptane, *Combustion and Flame*, Volume 128, Issue No. 1-2, pp. 38-59.
- [33] Ciezki, H., Adomeit, G. 1993. Shock-Tube Investigations of Self-Ignition of n-Heptane-Air Mixtures Under Engine Relevant Conditions, *Combustion and Flame*, Volume 93, Issue No. 4, pp. 421-433.
- [34] Pfahl, U., Fieweger, K., Adomeit, G. 1996. Self-ignition of diesel-relevant hydrocarbon-air mixtures under engine conditions, *Twenty Sixth Symposium (International) on Combustion/The Combustion Institute*, Pittsburgh, PA, USA.
- [35] Pischinger, R. 1968. *Bombenversuche über Gasverbrennungen*, Habilitation Thesis, Technische Hochschule Graz, Graz, Austria, pp. 61ff and Bildband pp. 134ff.
- [36] Schlatter, S., Schneider, B., Wright, Y., Boulouchos, K. 2012. Experimental Study of Ignition and Combustion Characteristics of a Diesel Pilot Spray in a Lean Premixed Methane/Air Charge using a Rapid Compression Expansion Machine, *SAE Technical Paper 2012-01-0825*.
- [37] Hanjalic, K., Popovac, M., Hadziabdic, M. 2004. A robust near-wall elliptic-relaxation eddy-viscosity turbulence model for CFD, *International Journal of Fluid Flow*, Volume 25, Issue No. 6, pp. 1047-1051.
- [38] Colin, O., Benkenida, A., Angelberger, C. 2003. 3D Modeling of Mixing, Ignition and Combustion Phenomena in Highly Stratified Gasoline Engines, *Oil Gas Science Technology*, Volume 58, pp. 47–62.
- [39] Colin, O., Benkenida, A. 2004. The 3-Zones Extended Coherent Flame Model (ECFM3Z) for Computing Premixed/Diffusion Combustion, *Oil Gas Science Technology*, Volume 59, pp. 593-609.
- [40] Eder, L., Kiesling, C., Pirker, G., Wimmer, A. 2017. Multidimensional Modeling of Injection and Combustion Phenomena in a Diesel Ignited Gas Engine, *SAE Technical Paper 2017-01-0559*.
- [41] Patankar, S., Spalding, D. 1972. A calculation procedure for heat, mass and momentum transfer in three-dimensional parabolic flows, *International Journal of Heat and Mass Transfer*, Volume 15, Issue No. 10, pp. 1787-1806.
- [42] Lin, S. 1954. Cylindrical Shock Waves Produced by Instantaneous Energy Release, *Journal of Applied Physics*, Volume 25.
- [43] Taylor, G. 1950. The Formation of a Blast Wave by a Very Intense Explosion. I. *Theoretical Discussion, Proceedings of the Royal Society of London. Series A, Mathematical and Physical Sciences*, Volume 201, pp. 159-174.
- [44] Eder, L., Kiesling, C., Pirker, G., Wimmer, A. 2017. Development and Validation of a Reduced Reaction Mechanism for CFD Simulation of Diesel Ignited Gas Engines, *XIII. Tagung zur Motorischen Verbrennung - ENCOM*, Ludwigsburg, Germany, pp. 241-252.